Imaging Agents

DOI: 10.1002/ange.201301135

Multi-Chromatic pH-Activatable ^{19}F-MRI Nanoprobes with Binary ON/OFF pH Transitions and Chemical-Shift Barcodes**

*Xiaonan Huang, Gang Huang, Shanrong Zhang, Koji Sagiyama, Osamu Togao, Xinpeng Ma, Yiguang Wang, Yang Li, Todd C. Soesbe, Baran D. Sumer, Masaya Takahashi, A. Dean Sherry, and Jinming Gao**

Magnetic resonance imaging (MRI) is a powerful non-invasive imaging technique that has greatly impacted basic biological research as well clinical diagnosis of cancer and other diseases.[1] Conventional MR contrast agents are T_1 (e.g. Gd-DTPA) or T_2-based (e.g. iron oxide), which cause significant longitudinal or transverse relaxation of protons, respectively.[2] Despite their success in many biological applications, one potential limitation is the lack of multi-chromatic features that allows for simultaneous detection of multiple signals. Recently, ^{19}F has received significant attention in MR imaging and spectroscopy studies.[3] Compared to ^{1}H-MRI, ^{19}F-MRI has little biological background owing to the low levels of endogenous fluorine in the body. Moreover, ^{19}F has 100% natural abundance and its gyromagnetic ratio (40.06 MHz/T) is second only to ^{1}H, which makes it more sensitive for detection over other nuclei.[3f]

Herein, we report on the development of "multi-colored" pH-activatable ^{19}F-MRI nanoprobes with tunable pH transitions. Recently, extensive efforts have been dedicated to the development of stimuli-responsive nanoprobes.[4] Various nanosystems that respond to pH,[5] enzymatic expression,[6] redox reaction,[7] temperature,[8] and light[9] have been reported. Among these stimuli, the pH stands out as an important physiological parameter that plays a critical role in both the intracellular (pH_i) and extracellular (pH_e) milieu.[10] For example, dysregulated pH was described as another hallmark of cancer, where a "reverse" pH gradient across the cell membrane is observed in cancer cells compared to normal cells.[11] A variety of different types of MRI agents have been reported for measuring pH values,[12] but all have a rather broad pH response which may limit the accuracy of the pH measurement, particularly when the pH perturbation in the pathological tissue is small. Moreover, it is often necessary to administer another pH-insensitive agent to correct for the contribution of agent concentration to obtain pH-sensitive signals, which makes the procedure complicated and difficult to perform.[13]

Herein we describe the development of pH-sensitive ^{19}F-MRI nanoprobes with a binary (ON/OFF) response to a specific, narrow pH transition (0.25 pH unit). We theorize that a collection of such nanoprobes where each pH transition is encoded with a specific ^{19}F signature will allow for a simple readout of environmental pH value through an "activation barcode". To demonstrate this proof of concept, we synthesized three ^{19}F-MRI nanoprobes with different pH transitions and ^{19}F-reporters (Scheme 1). Through these nanoprobes, we show in phantom studies the feasibility of using either ^{19}F NMR spectroscopy or imaging to discriminate the pH differ-

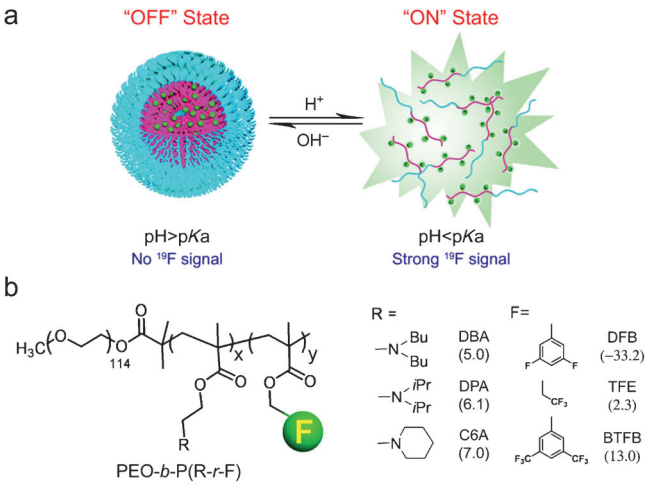

Scheme 1. a) pH-activatable ON/OFF ^{19}F-MRI nanoprobes from ionizable diblock copolymers. At $pH > pK_a$, the hydrophobic segments self-assemble into a micelle core leading to ^{19}F signal suppression as a result of restricted polymer chain motion. Upon pH activation ($pH < pK_a$), micelle disassembly leads to dissociated unimers and a strong ^{19}F signal. b) Structural formula of three representative diblock copolymers containing different pH responsive segments and ^{19}F reporter moieties, their pK_a values and ^{19}F chemical shifts (in ppm, relative to trifluoroacetic acid, or TFA), respectively, are shown in parenthesis.

[*] Dr. X. Huang, Dr. G. Huang, Dr. X. Ma, Dr. Y. Wang, Y. Li, Prof. J. Gao
Department of Pharmacology, Harold C. Simmons Comprehensive Cancer Center, UT Southwestern Medical Center at Dallas
5323 Harry Hines Blvds, Dallas, TX 75390 (USA)
E-mail: jinming.gao@utsouthwestern.edu
Dr. S. Zhang, Dr. K. Sagiyama, Dr. O. Togao, Dr. T. C. Soesbe, Prof. M. Takahashi, Prof. A. D. Sherry
Advance Imaging Research Center
UT Southwestern Medical Center at Dallas
5323 Harry Hines Blvds, Dallas, TX 75390 (USA)
Dr. B. D. Sumer
Department of Otolaryngology, UT Southwestern Medical Center at Dallas, 5323 Harry Hines Blvds, Dallas, TX 75390 (USA)

[**] This work is supported by the NIH (R01CA129011, R01EB013149). We acknowledge the assistance of the Southwestern Small Animal Imaging Resource, which is supported in part by NCI U24 CA126608, the Simmons Cancer Center through an NCI Cancer Center Support Grant (P30 CA142543).

Supporting information for this article is available on the WWW under http://dx.doi.org/10.1002/anie.201301135.

ences in the microenvironment (i.e. pH = 7.4, 6.5, 5.5, and 4.5).

The challenge in designing a set of multi-colored pH-activatable ^{19}F-nanoprobes is two-fold: first is the availability of reporter molecules that can be distinguished by MRS/I. For this purpose, ^{19}F is highly advantageous over ^{1}H probes as many ^{19}F reporter molecules have diverse chemical shifts and narrow peak widths that can be easily differentiated. The second is to devise an activation mechanism in which the signal intensities of these ^{19}F reporter molecules are highly responsive to the pH changes in the environment. In this regard, we adopted a strategy of using changes in spin–spin relaxations between the micelle and unimer states to turn ON/OFF ^{19}F signals in response to the pH value.[3e,i] ^{19}F reporters are introduced to the ionizable block (PR) of amphiphilic copolymers consisting of a hydrophilic poly(ethylene oxide) (PEO) segment and tertiary amine/ammonium segment (Scheme 1b). We hypothesize that at pH > pK_a, hydrophobic micelle assembly results in highly restricted chain motions and short spin–spin relaxation times ($T_2 \rightarrow 0$) to effectively broaden and eliminate the ^{19}F signals; at pH < pK_a, protonation of ammonium groups will result in micelle disassembly, conformational flexibility in the dissociated polymer chains (unimers), and reappearance of the previous ^{19}F signal.

For initial development, we synthesized the poly-(ethylene oxide)-*b*-poly[2-(diisopropylamino) ethyl methacrylate-*r*-trifluoroethyl methacrylate] (PEO-*b*-P(DPA-*r*-TFE)) copolymer using atom transfer radical polymerization method.[14] To investigate the optimal composition, we synthesized a series of PEO-*b*-P(DPA-*r*-TFE) copolymers with increasing molar ratios (5 to 75 mol%) of the TFE component (Table S1–S2, Figure S1 in the Supporting information). A higher TFE content should lead to more intense ^{19}F signals, whereas too much TFE may override the pH response from the DPA segment and induce micelle aggregation even at low pH values. Gel permeation chromatography (GPC) and ^{1}H NMR characterization demonstrated that all the copolymers had similar molecular weights ($1.5–1.8 \times 10^4$ Da) and polydispersity (Table S1, Figure S1). pH titration of the copolymers showed that the TFE content had a considerable influence on the pK_a and pH response of the copolymers. At 5 mol% of TFE, the pK_a is 6.3, similar to the PEO-*b*-PDPA copolymer without TFE.[5c] An increase in TFE content decreased the pK_a of the copolymers (Figure S2a). Based on these pK_a values, we chose pH 4.0 (below the pK_a values of all the copolymers) to evaluate the effect of TFE content on the ^{19}F signal intensity ($\delta_F = 2.3$ ppm for TFE relative to TFA). The ^{19}F signal intensity as a function of TFE content showed a bell-shaped response curve, where it reached a maximum at 40 mol% TFE. At pH 4.0, dynamic light scattering (DLS) experiments showed that all the copolymers except the PEO-*b*-P(DPA_{16}-*r*-TFE_{44}) (73 mol%) were in the unimer state as indicated by their small size (under 10 nm in diameter; Figure S2c). Whereas the PEO-*b*-P(DPA_{16}-*r*-TFE_{44}) copolymer formed micelles with a hydrodynamic diameter of 44 nm despite most of the amino groups being protonated at this pH value. The decrease of ^{19}F intensity can be explained by the rapid increase of spin–spin relaxation (or decreased T_2) at higher molar fraction of TFE (Figure S2e). Data show the T_2 is relatively unchanged (over 40 ms) when the TFE content is below 20 mol%. Based on these data, we chose 20 mol% (i.e. PEO-*b*-P(DPA_{48}-*r*-TFE_{12}) as the optimal ^{19}F-reporter composition in subsequent pH response studies.

^{19}F NMR spectra of PEO-*b*-P(DPA_{48}-*r*-TFE_{12}) copolymer collected as a function of pH demonstrate ultra-pH responsive behavior (Figure 1), similar to previously reported

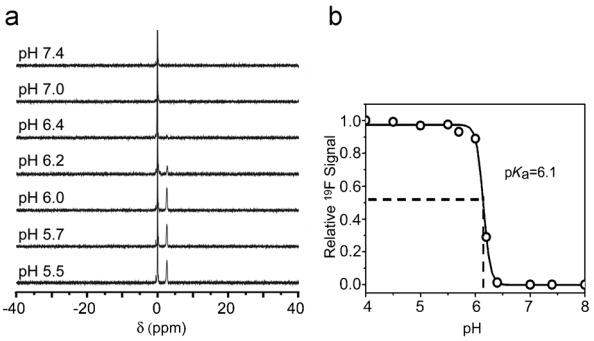

Figure 1. a) ^{19}F spectra of 2 mg mL^{-1} PEO-*b*-P(DPA_{48}-*r*-TFE_{12}) micelles in deuterated acetate buffers at different pH values. TFA was used as an external reference with its chemical shift set as 0. b) Normalized ^{19}F signal intensity as a function of pH value. Data was obtained from (a).

fluorescent nanoparticles.[5c,d] Below pH 6.0, we observed complete activation of ^{19}F signals; above pH 6.2, the ^{19}F signals largely disappeared. The pH difference ($\Delta pH_{10–90\%}$) between 10 to 90% signal difference is 0.25 pH units. This ultra-pH response is a unique property of this class of ionizable amphiphilic block copolymers, where hydrophobicity-driven micellization dramatically increased the cooperative deprotonation of the ammonium blocks.[5c,d] Transmission electron microscopy (TEM) of PEO-*b*-P(DPA_{48}-*r*-TFE_{12}) verified the formation of micelles at pH 7.4 (above its pK_a of 6.1) and complete micelle dissociation at pH 5.0 (Figure S3a). The micelle–unimer transition was further corroborated by ^{1}H NMR spectroscopy (Figure S3b) and dynamic light scattering, which showed the hydrodynamic diameters were changed from 40 to 6 nm at pH 7.4 and 5.0, respectively (Figure S3c).

To investigate the ON/OFF pH-activatable MR imaging capability of the nanoprobes, we prepared a sample in two concentric tubes where both tubes were filled with PEO-P(DPA_{48}-*r*-TFE_{12}) at 25 mg mL^{-1} but the pH values of the inner and outer tubes were set at 5.0 and 7.4, respectively. Axial ^{1}H MRI images showed two compartments with similar signal intensities (left panel, Figure 2a). In contrast, the corresponding ^{19}F MRI images showed an intense signal (ON) in the inner tube but no signal (OFF) in the outer tube (right panel, Figure 2a). We quantified the signal intensity in different regions of interest (ROI) over the background noise (Figure 2b). At 55 min, the ^{19}F signal-to-noise ratio (SNR) reached 31-fold for the PEO-*b*-P(DPA_{48}-*r*-TFE_{12}) nanoprobes at pH 5.0 (ON state). Then we compared the contrast of ^{19}F images between the ON and OFF states at pH 5.0 and 7.4, respectively. The contrast ratio ($SNR_{pH5.0}$/

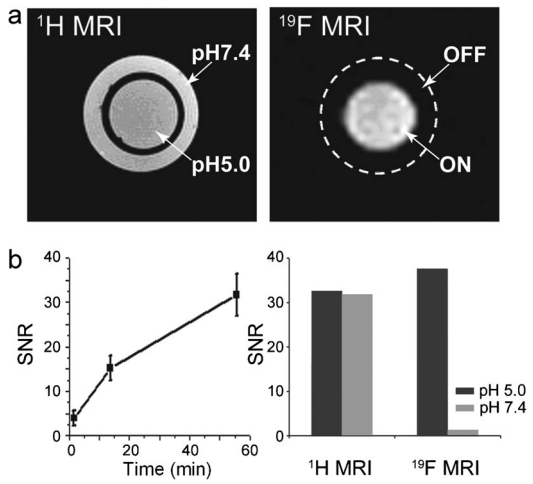

Figure 2. a) ^{1}H and ^{19}F MRI images of PEO-*b*-P(DPA$_{48}$-*r*-TFE$_{12}$) (25 mg mL^{-1}) phantom at pH 5.0 (inner tube) and 7.4 (outer tube). b) SNR of ^{19}F signals for PEO-*b*-P(DPA$_{48}$-*r*-TFE$_{12}$) as a function of scanning time at pH 5.0 (left panel) and comparison of SNR ratios at pH 5.0 and 7.4 from both ^{1}H and ^{19}F MRI images (right).

$SNR_{pH7.4}$) is 27-fold based on the ^{19}F images, demonstrating that the ^{19}F reporters on the polymers are highly responsive to the pH changes in the environment. In comparison, the $SNR_{pH5.0}/SNR_{pH7.4}$ ratio from the ^{1}H images was only 1.2.

Finally, we investigated the "barcode" concept using a mixture of ^{19}F-MRI nanoprobes with different pH transitions and ^{19}F reporter molecules to distinguish pH values in the microenvironment. In addition to TFE ($\delta_F = 2.3$ ppm), we introduced two additional ^{19}F reporter molecules (Scheme 1 b, DFB and BTFB, $\delta_F = -33.2$ and 13.0 ppm, respectively). These reporter molecules were incorporated into two new copolymers with different pH sensitivities, poly(ethylene oxide)-*b*-poly[2-(pentamethylene imino) methacrylate-*r*-2-(methacryloyloxy) ethyl 3,5-bis(trifluoromethyl) benzoate] (PEO-*b*-P(C6A-*r*-BTFB)) and poly(ethylene oxide)-*b*-poly[2-(dibutylamino) methacrylate-*r*-2-(methacryloyloxy) ethyl 3,5-difluorobenzoate] (PEO-*b*-P(DBA-*r*-DFB); Table S3). pH titration experiments demonstrated similar ultra-pH responsive properties of the two new copolymers (Figure S4). The pK_a values of the PEO-*b*-P(C6A-*r*-BTFB) and PEO-*b*-P(DBA-*r*-DFB) copolymers were 7.0 and 5.0, respectively, in addition to PEO-*b*-P(DPA-*r*-TFE) (pK_a = 6.1). Based on these pK_a values, we defined a three-digit barcode where each digit corresponds to one nanoprobe (with pK_a from low to high), and has a binary response (1 for ON, 0 for OFF). For better visual demonstration, we also assigned a single color to each nanoprobe for the ON state (black for the OFF state). Such a barcode design allows for the direct readout of the microenvironment pH value within two adjacent pK_a values in which one nanoprobe is ON and the other is OFF (Figure 3 a).

To validate this concept, we performed a double blind experiment, in which four solutions at pH 7.4, 6.5, 5.5, and 4.5 were first prepared containing the same mixture of the three nanoprobes. ^{19}F spectroscopy was then performed for each solution. Figure 3 b shows a clearly distinguished barcode pattern of nanoprobe activation. More specifically, the (000) solution corresponds to the solution at pH 7.4, in which all the nanoprobes were OFF. Accordingly, the (001), (011), and (111) solutions correspond to solutions with pH values at 6.5, 5.5 and 4.5, respectively. The nanoprobe barcodes successfully distinguished the solution pH values. Lastly, addition of fetal bovine serum (5 or 10%) to the nanoprobe solutions at pH 4.5 did not affect the signal contrast significantly, demonstrating successful ^{19}F detection in biologically relevant media (Figure S5).

In addition to ^{19}F spectroscopy, we also used ^{19}F MRI to spatially resolve the nanoprobe activation map. A phantom sample was prepared in which four smaller tubes (each containing the same nanoprobe mixture in solutions at pH 7.4, 6.5, 5.5, and 4.5) were placed in a bigger tube with water only. T_1-weighted ^{1}H MRI images show similar signal intensity from all the tubes and the surrounding water (Figure 3 c). For ^{19}F MR imaging, we selectively activated each ^{19}F reporter at its chemical shift to examine the nanoprobe activation. Based on results from each ^{19}F channel, we were able to obtain the barcode information for the different regions of interest (Figure 3 c). Potentially, by combining the ^{19}F spectroscopy and imaging capabilities, we can generate a pH map where each voxel can be encoded with an activation barcode to indicate its environmental pH value with spatial discrimination.

In summary, we report the feasibility of a series of multichromatic pH-activatable ^{19}F nanoprobes encoded with different ^{19}F reporters at specific pH transitions. Compared to small molecular pH sensors (typically 2 pH unit for a 10-fold signal change across pK_a), the pH response of these nanoprobes is extremely sharp ($\Delta pH_{ON/OFF} \approx 0.25$ pH unit) and can be used as binary indicators for a specific pH transition. The current three nanoprobe collection provides the proof of concept and allows for a qualitative measurement of environmental pH values. This nanoplatform can potentially overcome the instrument complexity and short T_1 limitation of the ^{13}C-based hyperpolarization probes.[15] Moreover, compared to chemical exchange saturation transfer (CEST) or ^{1}H agents with which small pH-dependent chemical shifts are quantified,[12c,16] the chemical shifts of ^{19}F reporters are widely separated and easily differentiated for binary readout and data processing. Development of additional nanoprobes with more refined pH transitions will be useful to narrow the pH transitions and improve the precision of the pH measurement. In addition, use of hybrid nanoparticles to include all ^{19}F-encoded polymers in one system could further unify pharmacokinetics and biodistribution during in vivo studies. Through a barcode map from ^{19}F-imaging spectroscopy, it is conceivable to generate a pH map in three dimensions. Along with these exciting potentials, one main challenge in subsequent preclinical translation of these nanoprobes is the relatively low detection sensitivity of ^{19}F-MRS/I. Optimization of MR scan time, pulse sequence or coil design should further improve the current detection limit (0.16 mg mL^{-1} ^{19}F). Image resolution can also be compromised to achieve higher detection sensitivity. Upon successful demonstration, the ^{19}F nanoprobes will add to the existing arsenal of pH sensors to measure tissue pH values, an important physiological param-

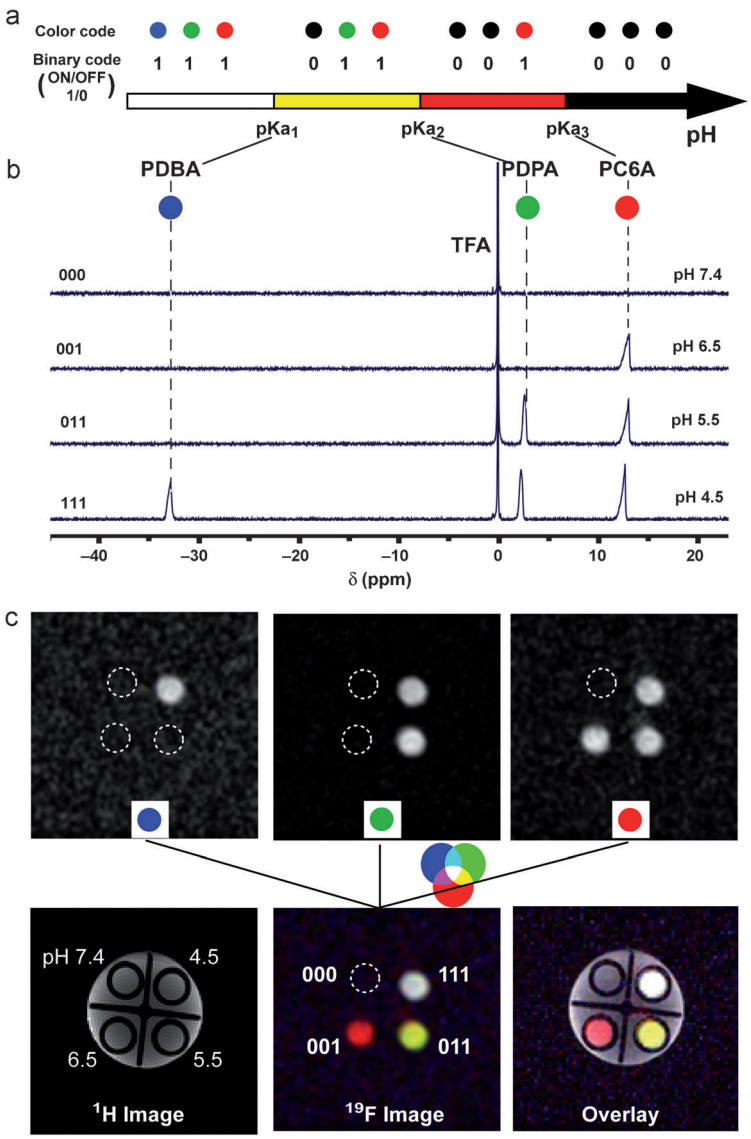

Figure 3. a) Schematic illustration of the activation barcode concept for direct readout of pH values between adjacent pK_a values. See text for details. b) ^{19}F spectra of a mixture of three PEO-*b*-P(R-*r*-F) nanoprobes in acetate buffers of different pH values. TFA was used as an external reference. c) ^{19}F MR imaging of the same nanoprobe mixture in solutions with different pH values. Detection of each ^{19}F reporter was accomplished by selective activation at its chemical shift (top panels). A "barcode map" (bottom middle panel) can be obtained by fusion of three ^{19}F reporter images. ^{19}F MR image was overlaid with ^{1}H image to show the spatial registration.

eter in many pathological indications (e.g. cancer, inflammation, and osteoporosis).

Received: February 7, 2013
Revised: March 26, 2013
Published online: June 20, 2013

Keywords: ^{19}F MRI · imaging agents · micelles · pH imaging · polymers

[1] a) P. Caravan, J. J. Ellison, T. J. McMurry, R. B. Lauffer, *Chem. Rev.* **1999**, *99*, 2293–2352; b) S. Laurent, D. Forge, M. Port, A. Roch, C. Robic, L. Vander Elst, R. N. Muller, *Chem. Rev.* **2008**, *108*, 2064–2110; c) S. G. Orel, M. D. Schnall, *Radiology* **2001**, *220*, 13–30.

[2] a) Y. W. Jun, J. H. Lee, J. Cheon, *Angew. Chem.* **2008**, *120*, 5200–5213; *Angew. Chem. Int. Ed.* **2008**, *47*, 5122–5135; b) C. Khemtong, C. W. Kessinger, J. Gao, *Chem. Commun.* **2009**, 3497–3510; c) C. Sun, J. S. Lee, M. Zhang, *Adv. Drug Delivery Rev.* **2008**, *60*, 1252–1265.

[3] a) J. M. Janjic, M. Srinivas, D. K. Kadayakkara, E. T. Ahrens, *J. Am. Chem. Soc.* **2008**, *130*, 2832–2841; b) Z. X. Jiang, X. Liu, E. K. Jeong, Y. B. Yu, *Angew. Chem.* **2009**, *121*, 4849–4852; *Angew. Chem. Int. Ed.* **2009**, *48*, 4755–4758; c) S. Mizukami, R. Takikawa, F. Sugihara, Y. Hori, H. Tochio, M. Walchli, M. Shirakawa, K. Kikuchi, *J. Am. Chem. Soc.* **2008**, *130*, 794–795; d) S. Mizukami, R. Takikawa, F. Sugihara, M. Shirakawa, K. Kikuchi, *Angew. Chem.* **2009**, *121*, 3695–3697; *Angew. Chem. Int. Ed.* **2009**, *48*, 3641–3643; e) M. Oishi, S. Sumitani, Y. Nagasaki, *Bioconjugate Chem.* **2007**, *18*, 1379–1382; f) J. Ruiz-Cabello, B. P. Barnett, P. A. Bottomley, J. W. Bulte, *NMR Biomed.* **2011**, *24*, 114–129; g) K. Tanaka, N. Kitamura, K. Naka, Y. Chujo, *Chem. Commun.* **2008**, 6176–6178; h) K. Yamaguchi, R. Ueki, H. Nonaka, F. Sugihara, T. Matsuda, S. Sando, *J. Am. Chem. Soc.* **2011**, *133*, 14208–14211; i) Y. Takaoka, T. Sakamoto, S. Tsukiji, M. Narazaki, T. Matsuda, H. Tochio, M. Shirakawa, I. Hamachi, *Nat. Chem.* **2009**, *1*, 557–561; j) J. X. Yu, R. R. Hallac, S. Chiguru, R. P. Mason, *Prog. Nucl. Magn. Reson. Spectrosc.* **2013**, *70*, 25–49; k) J. X. Yu, V. D. Kodibagkar, W. Cui, R. P. Mason, *Curr. Med. Chem.* **2005**, *12*, 819–848.

[4] a) E. S. Lee, Z. Gao, Y. H. Bae, *J. Controlled Release* **2008**, *132*, 164–170; b) V. Torchilin, *Eur. J. Pharm. Biopharm.* **2009**, *71*, 431–444.

[5] a) Y. Bae, S. Fukushima, A. Harada, K. Kataoka, *Angew. Chem.* **2003**, *115*, 4788–4791; *Angew. Chem. Int. Ed.* **2003**, *42*, 4640–4643; b) D. M. Lynn, M. M. Amiji, R. Langer, *Angew. Chem.* **2001**, *113*, 1757–1760; *Angew. Chem. Int. Ed.* **2001**, *40*, 1707–1710; c) K. Zhou, H. Liu, S. Zhang, X. Huang, Y. Wang, G. Huang, B. D. Sumer, J. Gao, *J. Am. Chem. Soc.* **2012**, *134*, 7803–7811; d) K. Zhou, Y. Wang, X. Huang, K. Luby-Phelps, B. D. Sumer, J. Gao, *Angew. Chem.* **2011**, *123*, 6233–6238; *Angew. Chem. Int. Ed.* **2011**, *50*, 6109–6114; e) E. S. Lee, K. Na, Y. H. Bae, *J. Controlled Release* **2003**, *91*, 103–113.

[6] a) A. Bernardos, E. Aznar, M. D. Marcos, R. Martinez-Manez, F. Sancenon, J. Soto, J. M. Barat, P. Amoros, *Angew. Chem.* **2009**, *121*, 5998–6001; *Angew. Chem. Int. Ed.* **2009**, *48*, 5884–5887; b) E. S. Olson, T. Jiang, T. A. Aguilera, Q. T. Nguyen, L. G. Ellies, M. Scadeng, R. Y. Tsien, *Proc. Natl. Acad. Sci. USA* **2010**, *107*, 4311–4316; c) C. Wang, Q. Chen, Z. Wang, X. Zhang, *Angew. Chem.* **2010**, *122*, 8794–8797; *Angew. Chem. Int. Ed.* **2010**, *49*, 8612–8615.

[7] a) Y. L. Li, L. Zhu, Z. Liu, R. Cheng, F. Meng, J. H. Cui, S. J. Ji, Z. Zhong, *Angew. Chem.* **2009**, *121*, 10098–10102; *Angew. Chem. Int. Ed.* **2009**, *48*, 9914–9918; b) G. Saito, J. A. Swanson, K. D. Lee, *Adv. Drug Delivery Rev.* **2003**, *55*, 199–215.

[8] a) S. W. Choi, Y. Zhang, Y. Xia, *Angew. Chem.* **2010**, *122*, 8076–8080; *Angew. Chem. Int. Ed.* **2010**, *49*, 7904–7908; b) B. Jeong, Y. H. Bae, S. W. Kim, *J. Controlled Release* **2000**, *63*, 155–163.

[9] a) A. G. Skirtach, A. Munoz Javier, O. Kreft, K. Kohler, A. Piera Alberola, H. Mohwald, W. J. Parak, G. B. Sukhorukov, *Angew. Chem.* **2006**, *118*, 4728 – 4733; *Angew. Chem. Int. Ed.* **2006**, *45*, 4612 – 4617; b) D. V. Volodkin, A. G. Skirtach, H. Mohwald, *Angew. Chem.* **2009**, *121*, 1839 – 1841; *Angew. Chem. Int. Ed.* **2009**, *48*, 1807 – 1809; c) S. Febvay, D. M. Marini, A. M. Belcher, D. E. Clapham, *Nano Lett.* **2010**, *10*, 2211 – 2219.

[10] B. Alberts, A. Johnson, J. Lewis, M. Raff, K. Roberts, P. Walter, *Molecular Biology of the Cell*, 5th ed., Garland Science, New York, **2008**.

[11] B. A. Webb, M. Chimenti, M. P. Jacobson, D. L. Barber, *Nat. Rev. Cancer* **2011**, *11*, 671 – 677.

[12] a) S. Aime, D. Delli Castelli, E. Terreno, *Angew. Chem.* **2002**, *114*, 4510 – 4512; *Angew. Chem. Int. Ed.* **2002**, *41*, 4334 – 4336; b) R. J. Gillies, N. Raghunand, G. S. Karczmar, Z. M. Bhujwalla, *J. Magn. Reson. Imaging* **2002**, *16*, 430 – 450; c) V. R. Sheth, Y. Li, L. Q. Chen, C. M. Howison, C. A. Flask, M. D. Pagel, *Magn. Reson. Med.* **2012**, *67*, 760 – 768; d) K. M. Ward, R. S. Balaban, *Magn. Reson. Med.* **2000**, *44*, 799 – 802; e) J. Zhou, J. F. Payen, D. A. Wilson, R. J. Traystman, P. C. van Zijl, *Nat. Med.* **2003**, *9*, 1085 – 1090; f) S. Zhang, K. Wu, A. D. Sherry, *Angew. Chem.* **1999**, *111*, 3382 – 3384; *Angew. Chem. Int. Ed.* **1999**, *38*, 3192 – 3194; g) Y. Wu, T. C. Soesbe, G. E. Kiefer, P. Zhao, A. D. Sherry, *J. Am. Chem. Soc.* **2010**, *132*, 14002 – 14003.

[13] a) M. L. Garcia-Martin, G. V. Martinez, N. Raghunand, A. D. Sherry, S. Zhang, R. J. Gillies, *Magn. Reson. Med.* **2006**, *55*, 309 – 315; b) N. Raghunand, C. Howison, A. D. Sherry, S. Zhang, R. J. Gillies, *Magn. Reson. Med.* **2003**, *49*, 249 – 257.

[14] a) N. V. Tsarevsky, K. Matyjaszewski, *Chem. Rev.* **2007**, *107*, 2270 – 2299; b) Y. H. Ma, Y. Q. Tang, N. C. Billingham, S. P. Armes, A. L. Lewis, A. W. Lloyd, J. P. Salvage, *Macromolecules* **2003**, *36*, 3475 – 3484.

[15] F. A. Gallagher, M. I. Kettunen, S. E. Day, D. E. Hu, J. H. Ardenkjaer-Larsen, R. Zandt, P. R. Jensen, M. Karlsson, K. Golman, M. H. Lerche, K. M. Brindle, *Nature* **2008**, *453*, 940 – 943.

[16] a) P. Provent, M. Benito, B. Hiba, R. Farion, P. Lopez-Larrubia, P. Ballesteros, C. Remy, C. Segebarth, S. Cerdan, J. A. Coles, M. L. Garcia-Martin, *Cancer Res.* **2007**, *67*, 7638 – 7645; b) M. T. McMahon, A. A. Gilad, M. A. DeLiso, S. M. Berman, J. W. Bulte, P. C. van Zijl, *Magn. Reson. Med.* **2008**, *60*, 803 – 812.